RESEARCH ARTICLE

A Novel α-Synuclein K58N Missense Variant in a Patient with Parkinson's Disease

Mohammed Al-Azzani, PhD,[1] Sandrina Weber, MD,[2] Nagendran Ramalingam, PhD,[3] Maria Ramón, MSc,[1] Liana Shvachiy, PhD,[1] Gonçalo Mestre, MSc,[1] Michael Zech, MD,[4,5,6] Kevin Sicking, PhD,[7,8] Alain Ibáñez de Opakua, PhD,[9] Vidyashree Jayanthi, BSc,[3] Leslie Amaral, PhD,[1,10] Aishwarya Agarwal, PhD,[11] Aswathy Chandran, PhD,[11] Susana R. Chaves, PhD,[10] Juliane Winkelmann, MD,[4,5,12,13] Claudia Trenkwalder, MD,[14,15] Maike Schwager, MSc,[16] Silke Pauli, PhD,[16] Ulf Dettmer, PhD,[3] Claudio O. Fernández, PhD,[17] Janin Lautenschläger, PhD,[11] Markus Zweckstetter, PhD,[9,18] Ruben Fernandez-Busnadiego, PhD,[7,8,19,20] Brit Mollenhauer, MD,[2,15*] and Tiago Fleming Outeiro, PhD[1,9,21,22*]

ABSTRACT: Background: Parkinson's disease (PD) is a complex multifactorial disorder with a genetic component in about 15% of cases. Multiplications and point mutations in *SNCA* gene, encoding α-synuclein (aSyn), are linked to rare familial forms of PD.

Objective: Our goal was to assess the clinical presentation and the biological effects of a novel K58N aSyn mutation identified in a patient with PD.

Methods: We describe the clinical presentation associated with the novel mutation, together with genetic

[1]University Medical Center Göttingen, Department of Experimental Neurodegeneration, Center for Biostructural Imaging of Neurodegeneration, Göttingen, Germany; [2]Department of Neurology, University Medical Center Göttingen, Göttingen, Germany; [3]Ann Romney Center for Neurologic Diseases, Brigham and Women's Hospital and Harvard Medical School, Boston, Massachusetts, USA; [4]Institute of Neurogenomics, Helmholtz Zentrum München, German Research Center for Environmental Health, Neuherberg, Germany; [5]Institute of Human Genetics, TUM School of Medicine and Health, Technical University of Munich, Munich, Germany; [6]Institute for Advanced Study, Technical University of Munich, Garching, Germany; [7]University Medical Center Göttingen, Institute for Neuropathology, Göttingen, Germany; [8]Aligning Science Across Parkinson's (ASAP) Collaborative Research Network, Chevy Chase, Maryland, USA; [9]German Center for Neurodegenerative Diseases, Göttingen, Germany; [10]CBMA–Centre of Molecular and Environmental Biology, School of Sciences, University of Minho, Braga, Portugal; [11]Cambridge Institute for Medical Research, University of Cambridge, Cambridge Biomedical Campus, Cambridge, United Kingdom; [12]Munich Cluster for Systems Neurology (SyNergy), Munich, Germany; [13]German Center for Mental Health (DZPG), partner site Munich-Augsburg, Munich-Augsburg, Germany; [14]Department of Neurosurgery, University Medical Centre Göttingen, Göttingen, Germany; [15]Paracelsus-Elena-Klinik, Kassel, Germany; [16]Institute of Human Genetics, University Medical Center Göttingen, Göttingen, Germany; [17]Max Planck Laboratory for Structural Biology, Chemistry and Molecular Biophysics of Rosario (MPLbioR, UNR-MPINAT), Partner Laboratory of the Max Planck Institute for Multidisciplinary Sciences (MPINAT, MPG). Centro de Estudios Interdisciplinarios, Universidad Nacional de Rosario, Rosario, Argentina; [18]Department for NMR-Based Structural Biology, Max Planck Institute for Multidisciplinary Sciences, Göttingen, Germany; [19]Cluster of Excellence "Multiscale Bioimaging: From Molecular Machines to Networks of Excitable Cells," University of Göttingen, Göttingen, Germany; [20]Faculty of Physics, University of Göttingen, Göttingen, Germany; [21]Translational and Clinical Research Institute, Faculty of Medical Sciences, Newcastle University, Newcastle Upon Tyne, United Kingdom; [22]Max Planck Institute for Multidisciplinary Sciences, Göttingen, Germany

*__Correspondence to:__ Prof. Dr. Tiago Fleming Outeiro, Experimental Neurodegeneration, Center for Biostructural Imaging of Neurodegeneration, University Medical Center Göttingen, Waldweg 33, 37073 Göttingen, Germany; E-mail: tiago.outeiro@med.uni-goettingen.de; Prof. Dr. Brit Mollenhauer, Department of Neurology, University Medical Center Göttingen, Robert-Koch-Straße 40, 37075 Göttingen, Germany; E-mail: brit.mollenhauer@med.uni-goettingen.de

Mohammed Al-Azzani and Sandrina Weber contributed equally to this work.

Relevant conflicts of interest/financial disclosures: Nothing to report.

Funding agencies: T.F.O. was supported by the Deutsche Forschungsgemeinschaft (DFG, German Research Foundation) under Germany's Excellence Strategy (EXC 2067/1–390729940) and by SFB1286 (B8). J.L. was supported by the Royal Society (Royal Society Dorothy Hodgkin Research Fellowship, DHF/R1/201228), the Addenbrooke's Charitable Trust (Grant 900325), the Leverhulme Trust (Research Project Grant RPG-2022-257), as well as a Career Support Fund from the University of Cambridge. L.S. was supported by the Foundation for Science and Technology (FCT, SFRH/BD/143286/2019). N.R. and U.D. were supported by the National Institutes of Health (Grants NS121826, NS099328, NS109209, AG085401, NS122880, and NS133979). M. Zweckstetter was supported by The Michael J. Fox Foundation (MJFF-022411). M. Zech acknowledges grant support by the European Joint Programme on Rare Diseases (EJP RD Joint Transnational Call 2022) and the German Federal Ministry of Education and Research (BMBF, Bonn, Germany), awarded to the project PreDYT (PREdictive biomarkers in DYsTonia, 01GM2302) by the Federal Ministry of Education and Research (BMBF) and the Free State of Bavaria under the Excellence Strategy of the Federal Government and the Länder, as well as by the Technical University of Munich–Institute for Advanced Study. M. Zech's research was supported by a "Schlüsselprojekt" grant from the Else Kröner-Fresenius-Stiftung (2022_EKSE.185). R.F.B. was supported by the DFG under Germany's Excellence Strategy (EXC 2067/1–390729940) and by SFB1286 (A12). Cryo-electron microscopy instrumentation at the University of Göttingen was jointly funded by the DFG Major Research Instrumentation program (448415290) and the Ministry of Science and Culture of the State of Lower Saxony. K.S. and R.F.B. were supported by the joint efforts of MJFF and the Aligning Science Across Parkinson's initiative; MJFF administers Grant ASAP-000282 on behalf of ASAP and itself.

Received: 13 June 2025; **Revised:** 11 August 2025; **Accepted:** 15 August 2025

Published online in Wiley Online Library (wileyonlinelibrary.com). DOI: 10.1002/mds.70030

testing through whole exome sequencing (WES). Furthermore, we conducted extensive biophysical and cellular assays to assess the functional consequences of this novel variant.

Results: The patient exhibited typical features of sporadic PD with early onset and a benign disease course. WES showed a novel heterozygous missense variant in *SNCA* (NM_000345.4, c.174G>C; p.K58N). A positive family history of PD was evident, because both a parent and a grandparent had been diagnosed with PD but were deceased. The patient underwent deep brain stimulation surgery 13 years postdiagnosis, showing stable, long-term improvements in motor symptoms. Biophysical studies demonstrated K58N substitution causes local structural effects, disrupts membrane binding, and enhances aSyn in vitro aggregation. In cellular systems, K58N aSyn produces fewer inclusions per cell and does not form condensates. The variant increases aSyn cytoplasmic distribution and displays aberrant activity-dependent dynamic serine-129 phosphorylation.

Conclusions: The clinical presentation associated with the novel K58N aSyn mutation suggests a relatively benign PD course consistent with the phenotypic spectrum of idiopathic PD. Overall, our molecular studies provide novel insight into the biology and pathobiology of aSyn. © 2025 The Author(s). *Movement Disorders* published by Wiley Periodicals LLC on behalf of International Parkinson and Movement Disorder Society.

Key Words: α-synuclein; Parkinson's disease; genetics; neurodegeneration; protein aggregation

Parkinson's disease (PD) is an age-associated neurodegenerative disorder classically manifesting with cardinal motor symptoms of tremor, rigidity, and bradykinesia, alongside nonmotor symptoms such as depression, autonomic dysfunction, and dementia.[1,2] Neuropathologically, PD involves progressive dopaminergic neuron degeneration in the substantia nigra and Lewy bodies (LBs), intraneuronal inclusions predominantly composed of aggregated α-synuclein (aSyn).[3-6] aSyn misfolding and aggregation occur in other synucleinopathies, such as dementia with LBs (DLB) and multiple system atrophy (MSA), with increasing evidence for distinct aSyn fibril structures within inclusions across synucleinopathies.[7-9]

aSyn, an intrinsically disordered protein, represents a significant focus of neuroscience research because of its central role in PD and related synucleinopathies, and its abundance and function in the nervous system. It is primarily concentrated in presynaptic terminals of neurons but is also present in other cellular compartments, including the nucleus, where it can interact with membranes adopting helical conformations and tetrameric structures.[10,11] Nevertheless, its precise physiological functions remain poorly understood, especially in non-neuronal cells.

In pathological conditions, aSyn misfolds and aggregates, disrupting cellular homeostasis and potentially causing neuronal death. Dopaminergic neurons in the substantia nigra are particularly vulnerable to these aggregates, although underlying mechanisms remain unclear. Although aSyn aggregation is often seen as the main driver of neurodegeneration, other theories suggest loss of functional monomeric aSyn because of aggregation (synucleinopenia) may contribute.[12,13] In reality, both proteinopathy and proteinopenia likely contribute to disease.

Pathogenic missense variants in *SNCA*, which encodes aSyn, cause familial PD forms, highlighting the importance of understanding their molecular effects to elucidate disease mechanisms. In fact, since the discovery of the first *SNCA* variant (A53T),[3] PD genetics has identified multiple additional *SNCA* variants and variants in other PD-related genes.[14,15] These aSyn variants include p.G14R, p.V15A, p.A30G, p.A30P, p.E46K, p.H50Q, p.G51D, p.A53T, p.A53E, p.A53V, and p.T72M, highlighting aSyn's central role in PD.[3,6,16-24] However, pathogenic SNCA variants are extremely rare, accounting for only 0.1% to 0.2% of cases.[14] SNCA duplications or triplications also cause familial PD.[25] SNCA triplications show a dose-dependent effect, causing early-onset, fully penetrant PD with severe nonmotor symptoms like depression, psychosis, and cognitive decline,[26,27] whereas duplications have variable presentations and are more often associated with DLB than PD.[26] Missense variants are generally rarer than duplications[15,28] and show a broad clinical spectrum, from idiopathic PD-like to atypical neurodegenerative phenotypes.[29] Notably, several heterozygous *SNCA* missense variants have been associated with milder clinical courses. The p.A30P and p.A30G substitutions often cause tremor-predominant PD with slow progression and long-preserved cognition, resembling idiopathic forms of PD.[6,22] Similarly, the p.H50Q variant shows reduced penetrance, with many heterozygous carriers remaining asymptomatic or developing mild, late-onset symptoms. These findings suggest that not all *SNCA* missense variants lead to a severe disease course, underscoring the importance of careful phenotypic documentation for new mutations. Consistently, our group recently described the novel p.G14R variant associated with an atypical, rapidly progressive phenotype and widespread neuronal loss combined with frontotemporal lobar degeneration–associated aSyn pathology.[24] To date, limited missense variants have been reported, with some having unresolved pathogenic relevance or requiring independent replication.[21,30,31] Their identification is further complicated by clinical heterogeneity

and incomplete penetrance,[16,32] resulting in negative family histories. Consequently, validating known variants and identifying novel ones are crucial for improving diagnostic accuracy and genetic counseling. Furthermore, these variants are also pivotal for research elucidating the molecular mechanisms underlying aSyn aggregation and its pathological/physiological properties, including phosphorylation at serine 129 (pS129).[33,34] For instance, different missense variants enhance or reduce aSyn pathological properties like aggregation and phosphorylation status.[24,35-37] Studying them is key to understanding both physiological and pathological roles of aSyn.

In this study, we identified a novel heterozygous SNCA missense variant in a familial PD case and comprehensively characterize its associated clinical phenotype and molecular effects.

Patients and Methods

Clinical Evaluation and Genetic Analysis

The patient was evaluated by movement disorder specialists at the tertiary movement disorder center Paracelsus Elena-Klinik, Kassel, Germany. Repeated general and neurological examinations included assessment of motor symptoms by Movement Disorder Society–revised Unified Parkinson's Disease Rating Scale (UPDRS), cognition by mini-mental status test (MMST), and standardized levodopa (L-dopa) challenge as described previously. Genetic analysis was performed, including whole exome sequencing (WES), to identify causative variants (details are provided in the Supporting Information). Written informed consent was obtained for participation in the genetic study in cooperation with the Institute of Human Genetics, Technical University Munich, Germany. The study was approved by the Ethics Commission of the Landesärztekammer Hessen, Frankfurt am Main, Germany (MC 284/2014). Additional consent was provided for confirmatory genetic testing at the Institute of Human Genetics, University Clinic Göttingen, Germany. Deep brain surgery was performed at the Clinic of Neurosurgery, University Medical Center Göttingen, Germany.

Biophysical and Cellular Studies

To understand how K58N mutation alters aSyn properties, we combined structural and cellular approaches. Recombinant protein was used for nuclear magnetic resonance (NMR) spectroscopy, Thioflavin T (ThT) aggregation assays, and cryo-electron microscopy (cryo-EM) to compare wild-type (WT) and K58N aSyn structure and fibril formation. Cellular models evaluated effects on aSyn aggregation, condensate formation, membrane association, and S129 phosphorylation. Full methods are provided in the Supporting Information.

Results

Clinical Presentation

The index patient, a white man, developed initial motor symptoms at approximately 39 years of age, with left-sided rest tremor, reduced arm swing, and mild bradykinesia. He was diagnosed with early-onset PD (EOPD) at the age of 42 years. Dopamine transporter imaging showed an asymmetrical reduction consistent with PD, with no clinical signs of atypical parkinsonism or other neurological disorders. After a good initial response to dopaminergic therapy, the patient developed motor fluctuations with end-of-dose wearing off, trunk dyskinesias in the *on* phase, and freezing of gait. Marked dystonia affected the left arm and leg. Thirteen years after PD diagnosis, he was evaluated for deep brain stimulation (DBS). At that time, nonmotor symptoms included excessive daytime sleepiness, fatigue, and depression. Neuropsychological assessment demonstrated no cognitive dysfunction, and a repeated MRI showed no abnormalities or features suggestive of atypical PD. Presurgical L-dopa challenge test demonstrated a robust response, with 78% improvement of UPDRS Part III. The patient received bilateral DBS of the subthalamic nucleus that reduced motor fluctuations, freezing, and tremor. At 3-year follow-up, motor symptom control remained good, with Mini Mental State Examination score 30/30 indicating preserved cognition, although moderate motor fluctuations reemerged. Family history was positive for PD in both a parent and a grandparent, who were deceased but reportedly showed no atypical features or dementia.

WES Identifies the p.K58N Missense Variant in aSyn

Given the early-onset of PD and positive family history, the patient underwent WES. WES identified a novel heterozygous missense variant in *SNCA* [NM_000345.4, c.174G>C; p.(K58N)] (Supporting Information Fig. S1A,-B). The variant was absent in the genomic databases gnomAD and the PD Variant Browser. It results in a lysine-to-asparagine substitution in a highly conserved region (Supporting Information Fig. S1C) and is predicted as deleterious by several in silico prediction algorithms (CADD:31, PolyPhen-2: 0.994, PrimateAI: 0.8337, REVEL: 0.653).

The Variant p.K58N Causes a Reduction in α-Helical Content, Impairing Its Interaction with Liposomes

To study the impact of the p.K58N variant on the structural and membrane-binding properties of aSyn, we employed NMR spectroscopy and Circular dichroism (CD) using recombinantly prepared monomeric

WT and K58N aSyn. The two-dimensional (2D) NMR $^{1}H/^{15}N$-correlation spectra for both proteins showed minimal signal, consistent with intrinsically disordered proteins (Fig. 1A). Most cross-peaks overlapped between the two variants, except for those near the mutation site (Fig. 1B–D). Chemical shift perturbations and intensity changes were restricted to the region surrounding the p.K58N substitution (Fig. 1B–D).

To investigate local conformation changes induced by the p.K58N variant, we calculated secondary structure propensity from NMR chemical shifts around the mutation site. Interestingly, the p.K58N variant showed a reduction in the α-helical content in this region (Fig. 1E). Furthermore, MD simulations of aSyn peptide G51-N65, either with WT lysine or mutant asparagine at position 58, reproduced NMR data of the full-length protein, showing decreased helical propensity in the mutant (Fig. 1F). Together, experimental and simulation findings demonstrate that p.K58N locally disrupts the α-helical structure (Fig. 1E,G).

Because aSyn adopts α-helical structures upon membrane binding, we assessed the impact of the p.K58N variant on this interaction by incubating aSyn with increasing amounts of liposomes and monitoring secondary structure transitions using CD spectroscopy.[38-40] Liposome exposure resulted in a shift from random coil into α-helical structure for both variants (Fig. 1H,I). However, the p.K58N variant displayed reduced ellipticity at 222 nm, indicating a lower propensity for α-helix formation, reflecting reduced liposome binding (Fig. 1J). These findings show α-helical content is reduced by the variant in a monomeric state, which may explain decreased liposome binding.

Effect of the Variant p.K58N on aSyn Aggregation In Vitro and Inclusions Formation in Cells

A central pathological hallmark in PD and other synucleinopathies is the accumulation of aSyn into insoluble aggregates. Therefore, we investigated whether the K58N substitution alters aSyn aggregation propensity. We first applied multiple prediction algorithms, which indicated increased β-strand content and higher aggregation tendency for K58N (Supporting Information Fig. S2).[41-43] Experimentally, recombinant WT and K58N aSyn were subjected to shaking-induced fibrillization, monitored by a ThT-based aggregation assay. Interestingly, the p.K58N variant showed a higher ThT aggregation profile and faster aggregation kinetics with a shorter $t_{1/2}$ compared with WT (Fig. 2A–D). These findings prompted us to further characterize fibrils by cryo-EM. As previously reported,[24] WT aSyn fibrils adopted two similarly populated conformations, one- (1PF) and two-protofilament (2PF) structures, respectively (Fig. 3A,C; Supporting Information Fig. S3). Three-dimensional (3D) reconstruction was successful only for 2PF fibrils, yielding a structure with 2.7 Å global resolution (Fig. 3E; Supporting Information Figs. S3 and S4) that enabled atomic model building. This model displays a double-arrow fold previously observed in other studies, such as "polymorph 2A" reported by Guerrero-Ferreira et al,[44] stabilized by a salt bridge between lysine 45 (K45) and glutamic acid 57 (E57) at the interprotofilament interface (Fig. 3G,H). The protofilament fold itself is nearly identical to those described as "polymorph L2A/B" by Frieg et al[45] and "protofilament fold B" by Lövestam et al.[46] However, in these cases, the interprotofilament interactions differ.

In contrast, the p.K58N variant adopted almost exclusively 2PF conformations (Fig. 3B,D; Supporting Information Fig. S5). A 3D reconstruction at 3.7 Å resolution enabled atomic modeling, demonstrating a protofilament fold similar to that of WT fibrils (Fig. 3F,I,J; Supporting Information Fig. S4). However, K58N fibrils present a higher twist (−1.29 degrees vs −0.81 degree in WT) and a slightly shifted protofilament interface, possibly because of the proximity of the K58N substitution to the interface-stabilizing residue (E57). In addition, no density for residues 14 to 25 was visible at the periphery of mutant fibrils (Fig. 3G–J). Altogether, these data indicate that the p.K58N variant displaces the conformational equilibrium of aSyn fibrils toward a 2PF structure reminiscent of that observed for WT.

Following the in vitro aggregation analysis, we explored whether the p.K58N variant exhibits altered aggregation behavior under a cellular environment, using the established SynT/Synphilin-1 (Sph1) model, a widely used cellular system for studying aSyn inclusions formation.[47] Human neuroglioma cells (H4) were cotransfected with WT or K58N SynT constructs and Sph1, followed by immunostaining 48 hours post-transfection. Interestingly, the K58N variant exhibited a significant decrease in the number and size of aSyn inclusions compared with WT (Fig. 2E–G) and an increased percentage of cells without inclusions compared with WT (Supporting Information Fig. S6).

K58N aSyn Shows Decreased Phase Separation

We further explored the impact of this novel variant on aSyn phase separation, a critical factor that is thought to play a role in its functional and pathological behavior. Under conditions promoting droplet formation, K58N aSyn exhibits markedly reduced droplet formation compared with WT aSyn (Fig. 4A). This is recapitulated at a quantitative scale, by turbidity assays in the presence of Ca^{2+} and varying Polyethylene glycol (PEG) concentrations (Fig. 4B).

We next expressed aSyn YFP with VAMP2 in HeLa cells, where VAMP2 induces aSyn phase separation

as previously shown.[48] In this study, WT aSyn YFP formed condensates, whereas K58N aSyn YFP failed to form condensates exhibiting a homogenous cytosolic distribution (Fig. 4C). Quantitative evaluation confirms the absence of condensate formation for the K58N aSyn variant (Fig. 4D).

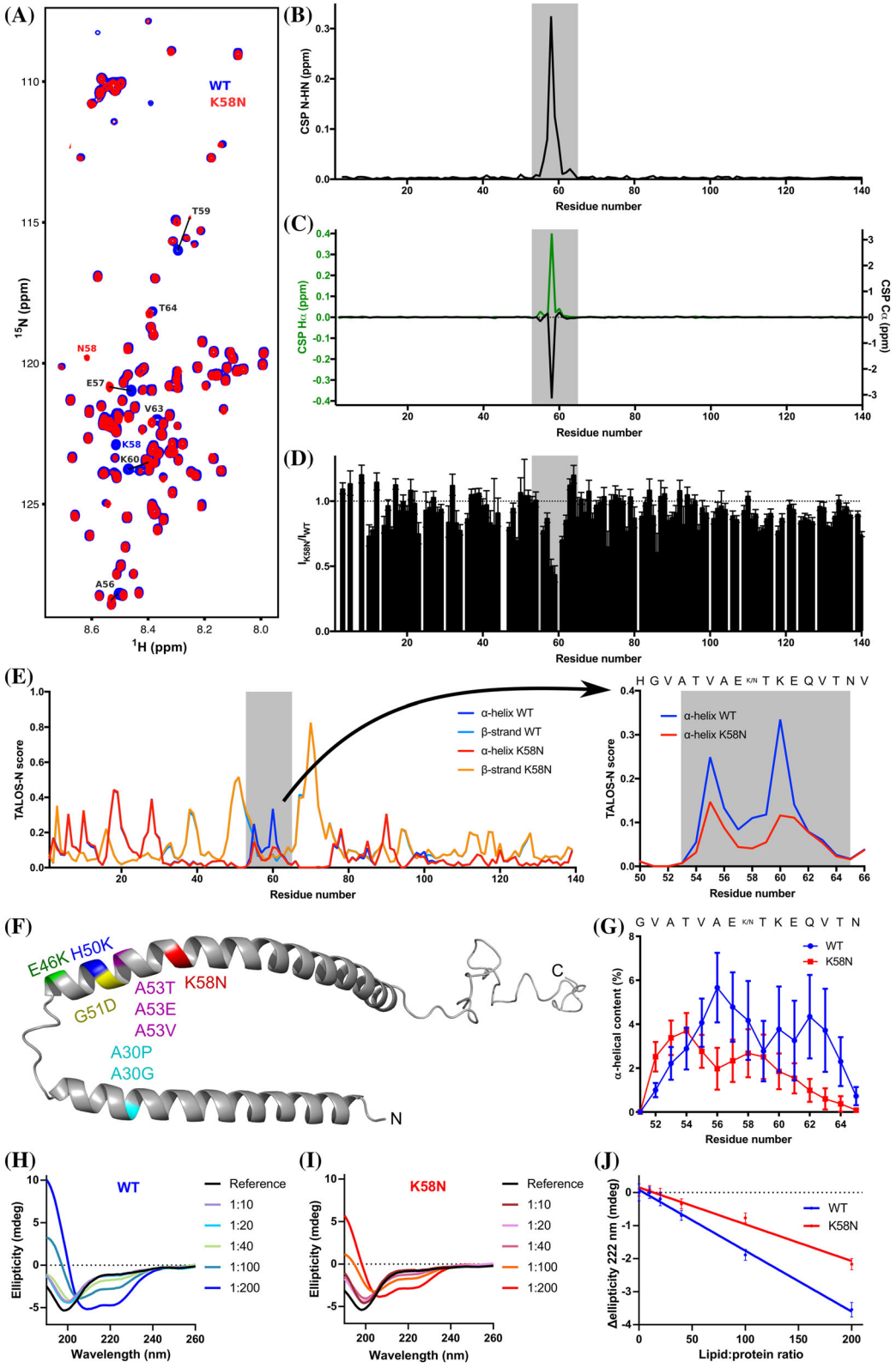

FIG. 1. Legend on next page.

Effects of the Variant p.K58N on aSyn pS129

There is increasing evidence that pS129 of aSyn is not only associated with pathology but also influences the physiological function of aSyn.[34] To investigate whether the p.K58N variant alters pS129 status, we employed lentiviral vectors to express either human WT or K58N aSyn in primary aSyn knockout (*SNCA*$^{-/-}$) rat cortical cultures (Fig. 5A). Under basal conditions (ie, without neuronal stimulation), K58N aSyn exhibited significantly reduced pS129 levels compared with WT (Fig. 5B). Recent studies showed familial PD-associated aSyn mutants with reduced membrane (M) localization often exhibit lower basal pS129 levels.[34] In line with this, we observed that the variant p.K58N was enriched in the cytosolic fraction (C) (GAPDH fraction, ~ 62%) (Fig. 5C,D), supporting the idea that reduced membrane association contributes to lower pS129 levels.

pS129 also has been recently reported to a dynamic, activity-dependent physiological process, where pS129

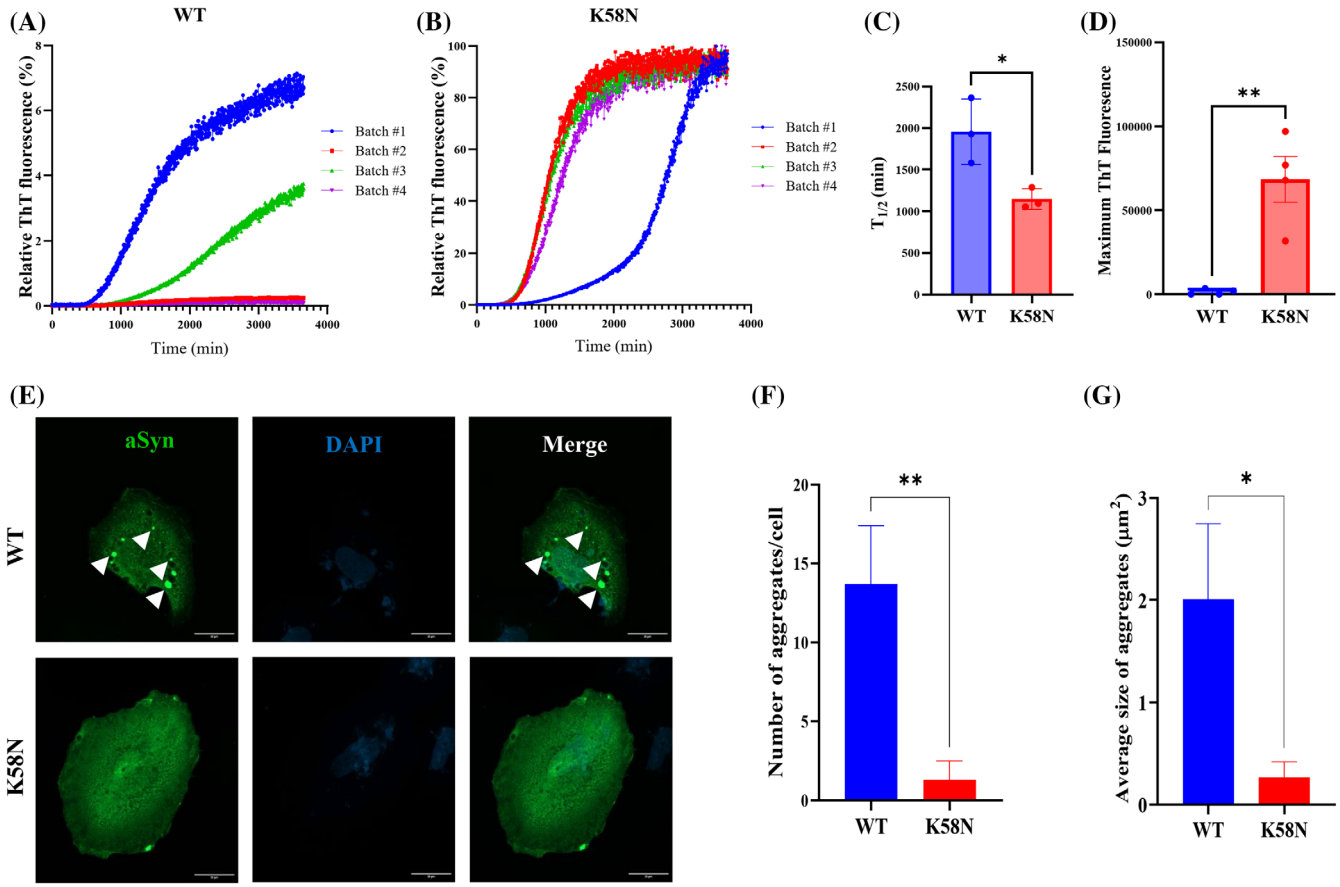

FIG. 2. K58N aSyn aggregation propensity. (**A–D**) In vitro ThT-based aggregation assays for wild type (WT) and K58N α-synuclein (aSyn). (**A** and **B**) Aggregation kinetic profiles of WT and K58N aSyn. Data were normalized to the maximum fluorescence value of each run. (**C**) Comparison of the half-time in minutes for aggregation kinetics. (**D**) Comparison of maximum ThT fluorescence values of WT and K58N. Error bars represent mean ± SD. (**E–G**) Effect of K58N mutation on inclusion formation in cells. The patterns of inclusions formation were investigated using the SynT/Sph1 aggregation model, which is based on the coexpression of WT or K58N SynT variants and Sph1. (**E**) Immunohistochemistry images representing the inclusion formation in H4 cells expressing WT and K58N aSyn. Scale bars, 20 μm. (**F**) Quantification of the number of inclusions per cell and their area (**G**). For each experiment, 50 cells were counted at 100× original magnification. The data analysis was performed using a Student's *t* test and presented as mean ± SD (N = 3). **P* < 0.05, ***P* < 0.01. [Color figure can be viewed at wileyonlinelibrary.com]

FIG. 1. The p.K58N variant decreases the α-helical content affecting liposome binding. (**A**) $^{1}H,^{15}N$ Heteronuclear Single-Quantum Coherence (HSQC) of α-synuclein (αSyn) wild type (WT) (blue) and K58N (red). Evident Chemical shift perturbation (CSPs) are labeled. (**B**) Combined HN/N CSPs generated by the K58N mutation over the αSyn sequence. (**C**) Affected region is highlighted in gray. Hα (green) and Cα (black) CSPs. (**D**) Normalized $^{1}H,^{15}N$ HSQC intensity ratios. Error bars are calculated from signal-to-noise ratios of individual resonances. (**E**) Secondary structure calculations from nuclear magnetic resonance (NMR) chemical shifts for αSyn WT (α-helix, blue; β-strand, light blue) and K58N (α-helix, red; β-strand, orange). On the right a zoom of the affected region with the α-helical content is plotted. (**F**) Micelle-bound αSyn structure (Protein Data Bank [PDB] ID: 1XQ8) with the positions of the different pathological mutations highlighted. (**G**) Residue-specific α-helical content over 100-ns MD simulations. Error bars indicate the standard error from 40 analyzed peptides. (**H–I**) CD experiments of WT (**H**) and K58N (**I**) αSyn at different protein/lipid ratios. (**J**) Ellipticity change at 222 nm on increasing concentrations of lipids for WT (blue) and K58N (red). More negative values indicate a bigger increase of α-helical structure. [Color figure can be viewed at wileyonlinelibrary.com]

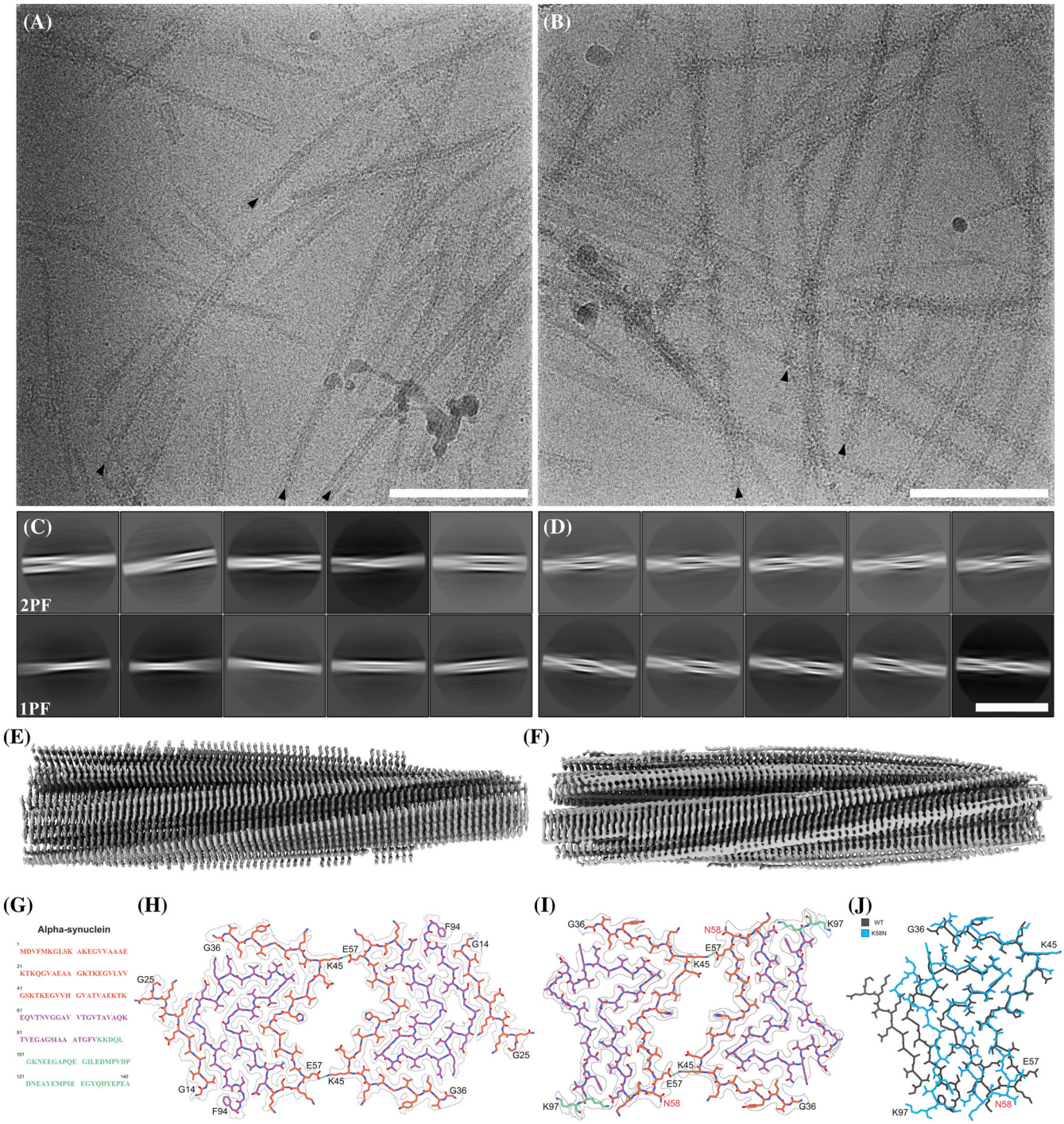

FIG. 3. Characteristics of wild-type (WT) and K58N α-synuclein (aSyn) filaments. (**A**) Transmission electron microscopy (TEM) micrograph of WT aSyn amyloid filaments. Black arrows mark selected filament ends. Scale bar, 100 nm. (**B**) TEM micrograph of K58N aSyn amyloid filaments. Black arrows indicate filament ends of exemplary filaments. Scale bar, 100 nm. (**C**) Two-dimensional (2D) class averages (706-Å box size) of twisting WT aSyn filaments, illustrating the interaction between either two protofilaments (2PF) or a single protofilament (1PF). (**D**) 2D class averages (706-Å box size) show twisting K58N aSyn filaments, again characterized by two protofilaments interacting with each other. Scale bar, 50 nm. (**E**) Overview of the electron density map of WT aSyn filaments. (**F**) Overview of the electron density map of K58N aSyn filaments. (**G**) Amino acid sequence of human aSyn with distinct regions color-coded (N terminus in orange, nonamyloid component in purple, and C terminus in green). (**H**) The electron density map together with the atomic model of WT aSyn amyloid filaments featuring a single beta-sheet layer formed by two interacting protofilaments. The protofilament interface is stabilized by a K45-E57 salt bridge. (**I**) The electron density map together with the atomic model of K58N aSyn amyloid filaments. The protofilament interface is again stabilized by the K45-E57 salt bridge. The mutated residue is indicated in red. (**J**) Superposition of the WT atomic model (gray) and the K58N mutant (blue). Although the double-arrow structure is similar, notable differences in the backbone highlight the impact of the K58N mutation (residue marked in red) on the overall aSyn filament structure. [Color figure can be viewed at wileyonlinelibrary.com]

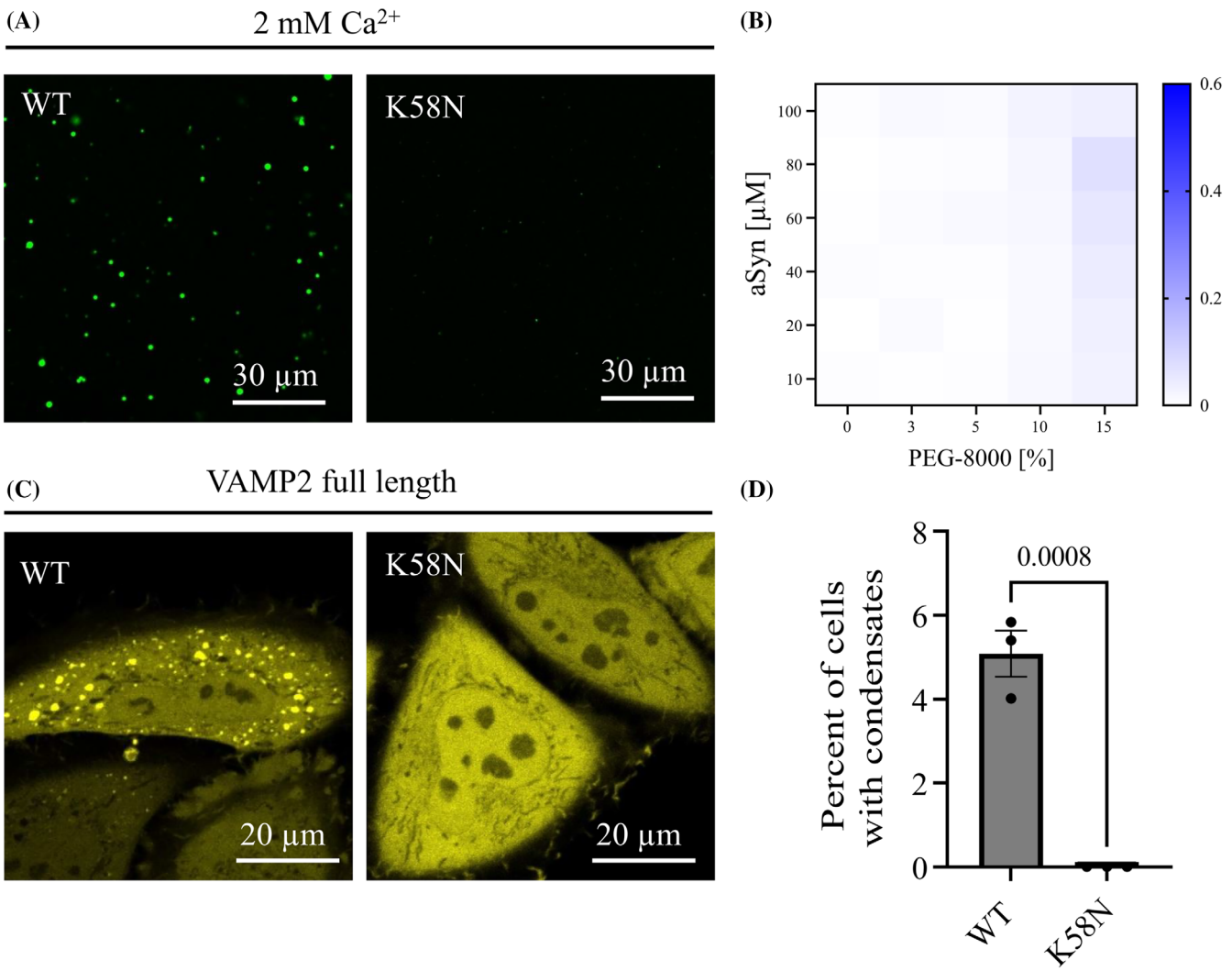

FIG. 4. aSyn K58N shows decreased condensate formation in vitro and in cells. (**A**) aSyn phase separation in the presence of 2 mM Ca^{2+} and crowding with 15% PEG-8000, immediately after PEG addition for aSyn wild-type (WT) and the disease variant aSyn K58N. aSyn concentration used: 100 µM. (**B**) Heatmap for turbidity measurements of aSyn phase separation in the presence of 2 mM Ca^{2+}. Data are derived from four independent repeats. (**C**) Condensate formation of aSyn WT YFP and aSyn K58N YFP on ectopic expression with VAMP2 in HeLa cells. aSyn K58N YFP does not undergo condensate formation in cells. (**D**) Quantification of condensate formation. Data were derived from incuCyte screening, 16 images per well, three wells per biological repeat, three biological repeats. n indicates biological repeats. Data are represented as mean ± SD. Unpaired two-tailed *t* test. [Color figure can be viewed at wileyonlinelibrary.com]

increases after neuronal stimulation and reversibly returns to baseline once the stimulus dampens or is inhibited.[34] Importantly, rodent neuron cultures expressing PD-associated A30P and E46K aSyn mutants showed impaired dynamic reversibility of pS129.[49] Therefore, we assessed the effect of K58N on activity-dependent pS129 dynamics by exposing WT or K58N aSyn transduced rat *SNCA*$^{-/-}$ cortical neurons at days in vitro (DIV) 17 to 21 to neuronal stimulation with picrotoxin (PTX; a GABA_A receptor antagonist), inhibition using tetrodotoxin (TTX; a sodium channel blocker), or a combination of stimulation followed by inhibition (Fig. 5E). Consistent with our previous observations, PTX exposure for 2 or 4 hours significantly increased pS129 in WT neurons, whereas TTX decreased basal pS129 by ~30%. TTX inhibition 2 hours after PTX stimulation effectively reversed activity-dependent pS129 elevation (Fig. 5F). K58N neurons followed a similar activity-dependent pS129 response (Fig. 5G); however, 4-hour PTX treatment induced a more pronounced pS129 increase in K58N neurons than in WT, relative to baseline (Fig. 5H). To assess pS129 dynamic reversibility, we compared pS129 levels after 4-hour PTX with midpoint TTX inhibition with those after 2- or 4-hour PTX alone. The percentage of irreversible pS129 after PTX/TTX was similar between K58N and WT neurons at 2 hours (Fig. 5K), but lower in K58N

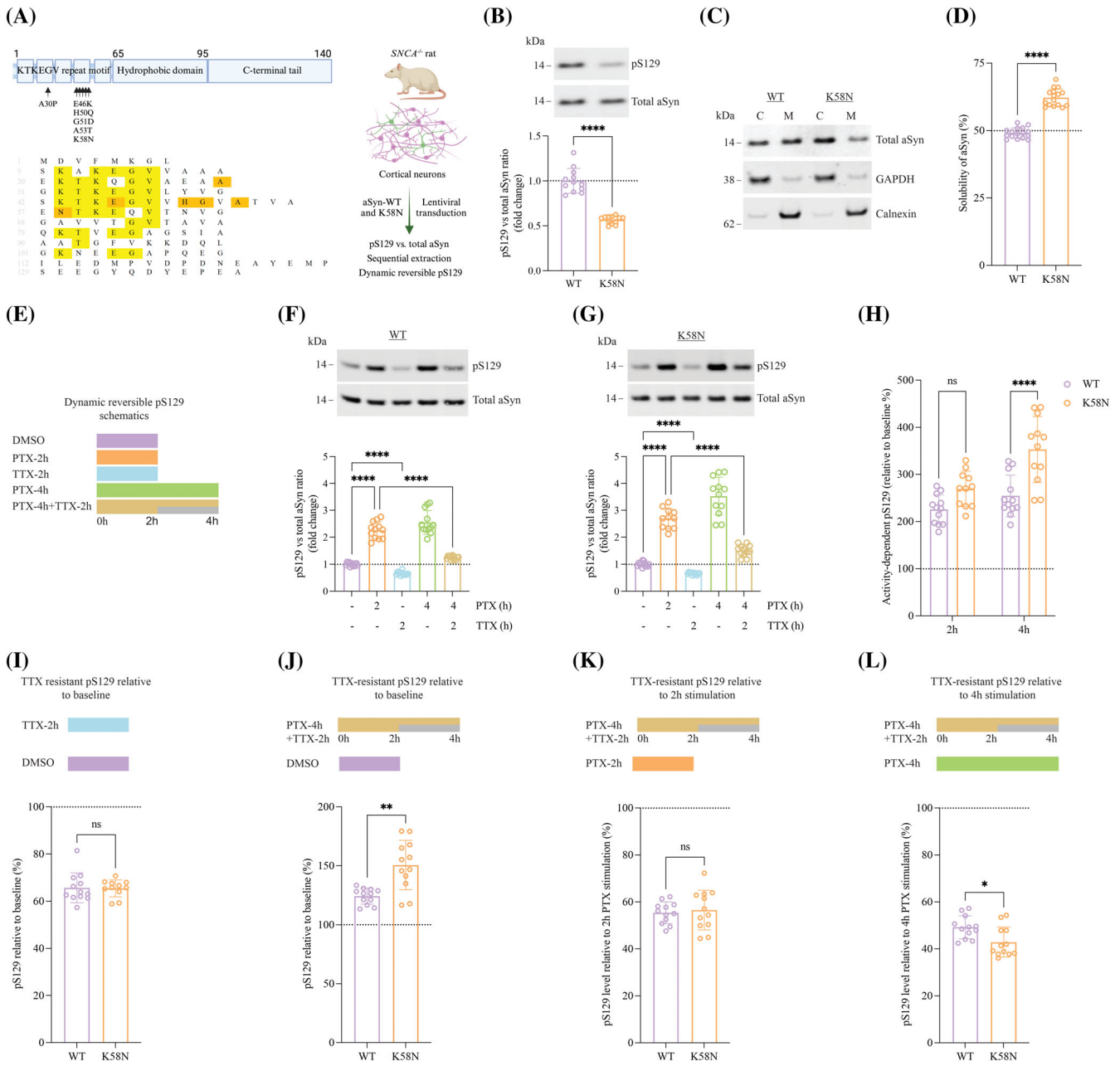

FIG. 5. Dynamic activity-dependent phosphorylation at serine 129 (pS129) of K58N and wild-type (WT) α-synuclein (aSyn). (**A**) Schematic illustration of aSyn structure exhibiting the KTKEGV repeat sequence harboring most familial PD mutations, central hydrophobic domain, and C-terminal region. The sequence alignment of aSyn is displayed below showing the conserved KTKEGV residues in yellow and sites of familial PD mutation in orange. On the right, the experimental setup is summarized. (**B**) A representative Western blot (WB) displaying the levels of total aSyn and pS129 from DIV 17–21 rat *SNCA*$^{-/-}$ cortical neurons expressing WT and K58N aSyn, with WB quantitative analysis presented below. (**C**) WB results of WT and K58N transduced rat *SNCA*$^{-/-}$ cortical neurons that were subjected to on-plate sequential extraction to isolate the cytosolic (C) and membrane (M) fractions. MJFR1 antibody was used for total aSyn detection, whereas GAPDH and Calnexin were used as cytosolic and membrane fractions controls, respectively. (**D**) Quantitative analysis of WT and K58N aSyn solubility from WB data in (**C**). (**E**) A summary of the experimental conditions to study pS129 dynamic reversibility, with more information provided in the main text. (**F** and **G**) Neuronal activity-dependent reversible phosphorylation of S129 (as outlined in **E**) was detected in DIV 17–21 rat *SNCA*$^{-/-}$ cortical neurons expressing WT or K58N, respectively, after picrotoxin (PTX) stimulation (20 μM) and tetrodotoxin (TTX) inhibition (1 μM). WB for quantifying total aSyn and pS129 was employed, and (**H**)–(**L**) are derived from (**F**) and (**G**). (**H**) The percentage of increase in pS129, compared with baseline, for WT and K58N aSyn observed after 2 or 4 h of PTX stimulation. (**I**) Comparison of TTX-resistant pS129 levels in WT and K58N variants relative to baseline conditions (DMSO vehicle). (**J**) The proportion of irreversible pS129 relative to the basal (DMSO vehicle) condition. (**K**) The proportion of irreversible pS129 relative to 2 h of PTX stimulation. (**L**) The proportion of irreversible pS129 relative to 4 h of PTX stimulation. ****$P < 0.0001$, ***$P < 0.001$, *$P < 0.05$. The error bar was mean ± SD. ns, not significant. [Color figure can be viewed at wileyonlinelibrary.com]

neurons after 4 hours (Fig. 5L). TTX inhibition under unstimulated conditions showed no significant difference between K58N and WT neurons (Fig. 5I). Overall, our findings indicate that activity-dependent pS129 dynamics are altered in K58N neurons, particularly after prolonged neuronal activity.

aSyn Containing the Variant p.K58N Is More Cytosolic without Changing Cytotoxicity in Yeast Cells

To investigate how the K58N aSyn variant affects cellular distribution and cytotoxicity, we used the well-established budding yeast model to associate subcellular localization with toxicity.[50] K58N aSyn predominantly localized to the cytoplasm, whereas WT aSyn formed cytoplasmic inclusions (Supporting Information Fig. S7A). Despite the different subcellular localization, the K58N and WT aSyn presented identical toxicities (Supporting Information Fig. S7).

Discussion

We report a novel *SNCA* missense variant (c.174G>C; p.K58N) and provide a detailed description of its clinical phenotype and molecular effects. The variant was identified through WES in a patient with EOPD and a positive family history, suggesting a genetic cause. Although both affected relatives were already deceased, DNA was unavailable for segregation analysis; the pathogenicity of the K58N is supported by its absence in genomic databases, disruption of a highly conserved residue, pathogenic predictions from multiple in silico tools, and critically, our molecular characterization results. According to ACMG (American College of Medical Genetics) guidelines,[51] p.K58N is classified as a variant of unknown significance. Our data now clarify its molecular consequences.

The clinical presentation and progression resembled idiopathic PD, with a good and sustained L-dopa response and the lack of motor and nonmotor symptoms indicating atypical PD. Both the parent and the grandparent were also diagnosed with PD; although both were already deceased and could not be examined, their medical history, as reported by the index patient, was consistent with idiopathic PD. Known pathogenic *SNCA* missense variants exhibit phenotypic spectrum ranging from typical idiopathic PD to atypical and more complex syndromes.[29] Atypical symptoms are common in patients with some variants such as p.G51D,[18,52] but rarely described in p.A30P and p.A30G,[22,53] which are associated with a more benign disease course compared with other missense variants, similar to our identified variant. However, unlike those variants, which often show early cognitive decline, no such symptoms were observed in this study. Motor fluctuations, common across all *SNCA* mutations including multiplications and observed in about two-thirds of cases,[26] were also present in the p.K58N patient and ultimately required the implantation of bilateral nucleus subthalamicus DBS. The intervention provided a good overall benefit for motor symptoms and motor fluctuations. Our study demonstrates DBS benefit in a p.K58N carrier, but recurrence of motor fluctuations after 4 years underscores the need for long-term follow-up. Emerging evidence indicates DBS outcomes may be affected by specific genetic mutations,[54] yet data on *SNCA* missense variants remain limited to a few cases and are inconsistent.[22,55-58] Although short-term motor improvement is consistently reported for DBS, two unrelated p.A53E patients experienced post-DBS progression for motor and nonmotor symptoms.[55,57] Reemergence of motor fluctuations after DBS was also reported in two patients with p.A30G variant (after 3 years)[22] and p.E46K (unknown interval),[58] but both had less aggressive progression than p.A53E cases. Additional data are needed to clarify how *SNCA* variants affect DBS outcomes, which is important for patient counseling and indication for DBS.

Most PD-associated aSyn variants occur in the N-terminal domain, a region crucial for interaction with lipids and biological membranes. Binding to membranes is mediated by KTKEGV repeats, which form amphipathic α-helices essential for lipid binding and key to aSyn structural and functional dynamics in cells. Under normal conditions, aSyn transitions between a cytosolic soluble disordered form and membrane-bound helical conformations.[40,59] N-terminal mutations often disrupt this balance by altering helical propensity, affecting membrane binding versus cytosolic solubility, and thus aSyn function and pathology.[47,60] The p.K58N variant is located in the N-terminal region, specifically within the KTKEGV motif, where lysine (K), a positively charged residue important for α-helix formation through electrostatics interactions with lipid headgroups in the membranes, is replaced by uncharged asparagine (N). This substitution is expected to disrupt α-helix structure and membrane binding.[61] Asparagine also favors turns and coils, potentially further destabilizing local structure. Consistently, our NMR data showed K58N mutation locally reduced α-helical content in residues A53–N65. Simulation data complemented the NMR findings, supporting disruption of aSyn helical propensity near the mutation site. The K58N-induced changes in conformational dynamics are expected to impact aSyn functional properties including its membrane interactions. However, the impact of PD-associated mutations on membrane binding varies and is further influenced by other factors such as membrane lipid composition and curvature. Among PD mutations, A30P is known to exhibit defective membrane binding by reducing helical propensity.[62,63] In this study, K58N reduced α-helical propensity in the presence of liposomes compared with WT aSyn, indicating a lower-affinity lipid-binding affinity.

A central hallmark of synucleinopathies is misfolding and aggregation of aSyn into insoluble, fibrillar protein deposits. Furthermore, distinct fibrils strains were reported across different synucleinopathies, prompting us to investigate p.K58N variant impact on aSyn

assembly. Importantly, this variant affects a residue adjacent to the central hydrophobic domain, a key region for aSyn aggregation. Furthermore, K58N local effects extended beyond the mutation site to residues farther away, including those at the start of the hydrophobic domain. Aggregation prediction algorithms suggest that K58N exhibits higher aggregation propensity, consistent with our in vitro aggregation assays showing increased ThT fluorescence and altered aggregation kinetics compared with WT aSyn. Substitution of positively charged K at position 58 with uncharged asparagine may remove protection against aggregation. This is reminiscent of the H50Q variant, where replacing partially charged histidine with neutral glutamine similarly increased aggregation tendency in vitro.[64,65]

The observed changes likely reflect distinct structural properties of fibrils formed by WT and K58N aSyn. Cryo-EM analysis demonstrated that p.K58N preferentially forms 2PF fibrils with a similar protofilament fold than WT fibrils, suggesting that the mutation stabilizes the WT interprotofilament interface. One possibility is that K58 modulates the ability of the adjacent interface-stabilizing residue (E57) to interact in *cis* or *trans*. In WT, K58 may form a salt bridge in *cis* with E57, potentially destabilizing the interprotofilament interface and thereby favoring 1PF structures. In contrast, the p.K58N variant may prevent this interaction because of the altered charge properties, thereby promoting *trans* interactions with K45 of an adjacent protofilament and thus favoring 2PF fibrils. Interestingly, this contrasts with our recent findings on the G14R mutation,[24] which promotes 1PF forms. Altogether, these results indicate that these mutations modulate the WT fibril conformational landscape, favoring either 1PF (G14R) or 2PF (K58N) forms.

In cells, K58N aSyn formed fewer and smaller inclusions compared with WT aSyn. This aligns with previous findings where some aSyn mutations showed attenuated aSyn aggregation in vitro but increased cellular inclusions.[24,47] The yeast model also showed a more diffuse cytoplasmic distribution for K58N, further demonstrating the importance of employing diverse experimental models when evaluating the effects of mutations in the behavior of aSyn, because this will likely uncover different properties of the protein.

aSyn phase separation forms dynamic condensates under physiological conditions,[66,67] but in certain pathological states, it can result in the formation of precursors or seeds that develop into solid, insoluble pathological aggregates.[68-70] Recent studies show that VAMP2 regulates aSyn phase separation condensate formation, likely through aSyn membrane interactions.[48,71] In these studies, A30P mutant, known for reduced lipid binding[61,72-74] and increased cytosolic localization,[50,75] failed to form condensates in cells. Interestingly, our assays showed that the K58N mutant also has impaired membrane binding and increased cytosolic distribution, similar to A30P.

The phosphorylation of aSyn at S129 (pS129), previously recognized as a pathological hallmark,[33] is increasingly recognized for its physiological role.[34,76] This phosphorylation is a dynamic reversible process regulated by neuronal activity, increasing with stimulation, and reversing when activity diminishes.[34] In our study, both WT and K58N aSyn exhibited similar activity-dependent pS129 patterns, aligning with previous findings for some PD-associated mutations.[24,49] These findings support mutation-specific pathological effects and align with the more benign disease course observed in the patient. These results underscore the importance of evaluating pS129 dynamics to better understand the molecular impact of aSyn mutations.

The identification and characterization of novel aSyn variants are very important for the field of synucleinopathies, because this not only sheds new light onto our understanding of pathological mechanisms, but it also enables the clinical stratification of patients (for clinical trials). In addition, this knowledge of disease-associated aSyn variants is important for genetic counseling, once the pathogenicity is confirmed, and may guide the application of potential future individualized therapies. ■

Author Roles: (1) Research Project: A. Conception, B. Organization, C. Execution; (2) Statistical Analysis: A. Design, B. Execution, C. Review and Critique; (3) Manuscript Preparation: A. Writing of the First Draft, B. Review and Critique.
M.A.: 1C, 2A, 2B, 2C, 3A, 3B.
S.W.: 1C, 2A, 2B, 3A, 3B.
N.R.: 1C, 2A, 2B, 2C, 3B.
M.R.: 1C, 3B.
L.S.: 1C, 3B.
G.M.: 1C, 3B.
M.Z.: 1C, 3B.
K.S.: 1C, 2B, 3B.
A.I.O.: 1C, 2B, 3B.
V.J.: 1C, 3B.
L.A.: 1C, 3B.
A.A.: 1C, 3B.
A.C.: 1C, 3B.
S.R.C.: 2B, 2C, 3B.
J.W.: 2C, 3B.
C.T.: 2C, 3B.
M.S.: 1C, 3B.
S.P.: 2C, 3B.
U.D.: 2A, 2C, 3B.
C.O.F.: 2C, 3B.
J.L.: 2A, 2C, 3B.
M.Z.: 2A, 2C, 3B.
R.F.B.: 2A, 2C, 3B.
B.M.: 1A, 1B, 2A, 2C, 3B.
T.F.O.: 1A, 1B, 2A, 2C, 3A, 3B.

Acknowledgments: T.F.O. was supported by the Deutsche Forschungsgemeinschaft (DFG, German Research Foundation) under Germany's Excellence Strategy (EXC 2067/1–390729940) and by SFB1286 (B8). J.L. was supported by the Royal Society (Royal Society Dorothy Hodgkin Research Fellowship, DHF/R1/201228), the Addenbrooke's Charitable Trust (Grant 900325), the Leverhulme Trust (Research Project Grant RPG-2022-257), as well as a Career Support Fund from the University of Cambridge. L.S. was supported by the Foundation for Science and Technology (FCT, SFRH/BD/143286/2019). N.R. and U.D. were supported by the National Institutes of Health (Grants NS121826, NS099328, NS109209, AG085401, NS122880, and NS133979). M. Zweckstetter was supported by The Michael J. Fox Foundation (MJFF-022411). M. Zech acknowledges grant support by the

European Joint Programme on Rare Diseases (EJP RD Joint Transnational Call 2022) and the German Federal Ministry of Education and Research (BMBF, Bonn, Germany), awarded to the project PreDYT (PREdictive biomarkers in DYsTonia, 01GM2302) by the Federal Ministry of Education and Research (BMBF) and the Free State of Bavaria under the Excellence Strategy of the Federal Government and the Länder, as well as by the Technical University of Munich–Institute for Advanced Study. M. Zech's research was supported by a "Schlüsselprojekt" grant from the Else Kröner-Fresenius-Stiftung (2022_EKSE.185). R.F.B. was supported by the DFG under Germany's Excellence Strategy (EXC 2067/1–390729940) and by SFB1286 (A12). Cryo-electron microscopy instrumentation at the University of Göttingen was jointly funded by the DFG Major Research Instrumentation program (448415290) and the Ministry of Science and Culture of the State of Lower Saxony. K.S. and R.F.B. were supported by the joint efforts of MJFF and the Aligning Science Across Parkinson's initiative; MJFF administers Grant ASAP-000282 on behalf of ASAP and itself. We thank Dr. Ellen Gerhardt for assistance with site-directed mutagenesis in the aSyn-encoding plasmids.

Financial Disclosures of All Authors: The authors report no financial disclosures or conflicts of interest for the past 12 months.

Data Availability Statement

The main data generated or analyzed during this study are included in this article (and its Supporting Information files). The micrographs used for the single-particle analysis (SPA) of aSyn fibrils are available in the EMPIAR database under accession code EMPIAR-12518. The atomic model and cryo-EM density map for the WT aSyn fibril are deposited in the Protein Data Bank (PDB) and Electron Microscopy Data Bank (EMDB) under accession codes 9HGS and EMD-52165, respectively. The corresponding data for the K58N mutant aSyn fibril are available under accession codes 9HXA (PDB) and EMD-52458 (EMDB). A comprehensive Key Resource Table, detailing datasets, software, and protocols, is available via Zenodo at: https://zenodo.org/records/14730688. In addition, the entry includes an Excel file with tabular data on the protofilament distribution of WT and K58N aSyn filaments, XML files containing tabular data for the FSC graphs of each density map used to determine the final resolution (generated with RELION 4.0), and two Python scripts for graphing the FSC XML data. The full single-particle analysis protocol describing the cryo-EM data processing strategy is available at Protocols.io (https://www.protocols.io/view/single-particle-analysis-of-synuclein-fibrils-81wgbxozylpk/v1).

References

1. Flores-Leon M, Outeiro TF. More than meets the eye in Parkinson's disease and other synucleinopathies: from proteinopathy to lipidopathy. Acta Neuropathol 2023;146:369–385.
2. Postuma RB, Berg D, Stern M, et al. MDS clinical diagnostic criteria for Parkinson's disease. Mov Disord 2015;30:1591–1601.
3. Polymeropoulos MH, Lavedan C, Leroy E, et al. Mutation in the α-synuclein gene identified in families with Parkinson's disease. Science 1997;276:2045–2047.
4. Spillantini MG, Schmidt ML, Lee VM, Trojanowski JQ, Jakes R, Goedert M. α-synuclein in Lewy bodies. Nature 1997;388:839–840.
5. Golbe LI, Di Iorio G, Bonavita V, Miller JC, Duvoisin RA. Clinical genetic analysis of Parkinson's disease in the Contursi kindred. Ann Neurol 1996;40:767–769.
6. Appel-Cresswell S, Vilarino-Guell C, Encarnacion M, et al. Alpha-synuclein p.H50Q, a novel pathogenic mutation for Parkinson's disease. Mov Disord 2013;28:811–813.
7. Schweighauser M, Shi Y, Tarutani A, et al. Structures of α-synuclein filaments from multiple system atrophy. Nature 2020;585:464–469.
8. Yang Y, Shi Y, Schweighauser M, et al. Structures of α-synuclein filaments from human brains with Lewy pathology. Nature 2022;610:791–795.
9. Scheres SHW, Ryskeldi-Falcon B, Goedert M. Molecular pathology of neurodegenerative diseases by cryo-EM of amyloids. Nature 2023;619:685–690.
10. Brás IC, Xylaki M, Outeiro TF. Mechanisms of alpha-synuclein toxicity: An update and outlook. Progress in Brain Research 2020;252:91–129.
11. Koss DJ, Erskine D, Porter AG, et al. Nuclear alpha-synuclein is present in the human brain and is modified in dementia with Lewy bodies. Acta Neuropathol Commun 2022;10:98.
12. Ezzat K, Sturchio A, Espay AJ. Proteins do not replicate, they precipitate: phase transition and loss of function toxicity in amyloid pathologies. Biology (Basel) 2022;11:1779.
13. Espay AJ, Lees AJ. Loss of monomeric alpha-synuclein (synucleinopenia) and the origin of Parkinson's disease. Parkinsonism Relat Disord 2024;121:106022.
14. Westenberger A, Klein C, Schulte C, et al. Relevance of genetic testing in the gene-targeted trial era: the Rostock Parkinson's disease study. Brain 2024;147:2652–2667.
15. Cook L, McLean JR, O'Connell K, et al. Parkinson's disease variant detection and disclosure: PD GENEration, a north American study. Brain 2024;147:2668–2679.
16. Daida K, Satake W, Iwasaki Y, et al. α-Synuclein V15A variant in familial Parkinson's disease exhibits a weaker lipid-binding property. Mov Disord 2022;37:1234–1240.
17. Krüger R, Kuhn W, Müller T, et al. Ala30Pro mutation in the gene encoding α-synuclein in Parkinson's disease. Nat Genet 1998;18:106–108.
18. Lesage S, Anheim M, Letournel F, et al. G51D α-synuclein mutation causes a novel parkinsonian-pyramidal syndrome. Ann Neurol 2013;73:459–471.
19. Yoshino H, Tomiyama H, Tachibana N, et al. Homozygous alpha-synuclein p.A53V in familial Parkinson's disease. Neurobiol Aging 2017;57:248.e7–248.e12.
20. Zarranz JJ, Alegre J, Gómez-Esteban JC, et al. The new mutation, E46K, of α-synuclein causes Parkinson and Lewy body dementia. Ann Neurol 2004;55:164–173.
21. Fevga C, Karantzelis N, Spanaki C, et al. A new alpha-synuclein missense variant (Thr72Met) in two Turkish families with Parkinson's disease. Parkinsonism Relat Disord 2021;89:63–67.
22. Liu H, Koros C, Strohäker T, et al. A novel SNCA A30G mutation causes familial Parkinson's disease. Mov Disord 2021;36:1624–1633.
23. Pasanen P, Myllykangas L, Siitonen M, et al. A novel α-synuclein mutation A53E associated with atypical multiple system atrophy and Parkinson's disease-type pathology. Neurobiol Aging 2014;35:2180.e1–2180.e5.
24. Brücke C, Lázaro DF, Ramalingam N, et al. A novel alpha-synuclein G14R missense variant is associated with atypical neuropathological features. medRxiv 2024. https://doi.org/10.1101/2024.09.23.24313864
25. Singleton AB, Farrer M, Johnson J, et al. α-Synuclein locus triplication causes Parkinson's disease. Science 2003;302:841.
26. Trinh J, Guella I, Farrer MJ. Genotype-phenotype relations for the Parkinson's disease genes SNCA, LRRK2, VPS35: MDSGene systematic review. Mov Disord 2018;33:1607–1616.
27. Konno T, Ross OA, Puschmann A, Dickson DW, Wszolek ZK. Autosomal dominant Parkinson's disease caused by SNCA duplications. Parkinsonism Relat Disord 2016;22(Suppl 1):S1–S9.
28. Blauwendraat C, Nalls MA, Singleton AB. A population scale analysis of rare SNCA variation in the UK biobank. Neurobiol Dis 2021;148:105210.

29. Petrucci S, Ginevrino M, Valente EM. Phenotypic spectrum of alpha-synuclein mutations: new insights from patients and cellular models. Parkinsonism Relat Disord 2016;22(Suppl 1):S16–S20.
30. Kapasi A, Dickson DW, Berger Z, et al. A novel SNCA E83Q mutation in a case of dementia with Lewy bodies and atypical frontotemporal lobar degeneration. Neuropathology 2020;40:76–85.
31. Blauwendraat C, Nalls MA, Singleton AB. Insufficient evidence for pathogenicity of SNCA His50Gln (H50Q) in Parkinson's disease. Neurobiol Aging 2018;64:159.e5–159.e8.
32. Papadimitriou D, Koros C, Stamelou M, et al. Motor and nonmotor features of carriers of the p.A53T alpha-synuclein mutation: a longitudinal study. Mov Disord 2016;31:1646–1650.
33. Fujiwara H, Hasegawa M, Dohmae N, et al. α-Synuclein is phosphorylated in synucleinopathy lesions. Nat Cell Biol 2002;4:160–164.
34. Ramalingam N, Brontesi L, Jin S, Selkoe DJ, Dettmer U. Dynamic physiological α-synuclein S129 phosphorylation is driven by neuronal activity. NPJ Parkinsons Dis 2023;9:4.
35. Li J, Uversky VN, Fink AL. Effect of familial Parkinson's disease point mutations A30P and A53T on the structural properties, aggregation, and fibrillation of human α-synuclein. Biochemistry 2001;40:11604–11613.
36. Fares MB, Ait-Bouziad N, Dikiy I, et al. The novel Parkinson's disease linked mutation G51D attenuates in vitro aggregation and membrane binding of α-synuclein, and enhances its secretion and nuclear localization in cells. Hum Mol Genet 2014;23:4491–4509.
37. Lázaro DF, Brás IC, Vasili E, et al. The effects of the novel A53E alpha-synuclein mutation on its oligomerization and aggregation. Acta Neuropathol Commun 2016;4:128.
38. Ulmer TS, Bax A, Cole NB, Nussbaum RL. Structure and dynamics of micelle-bound human α-synuclein. J Biol Chem 2005;280:9595–9603.
39. Davidson WS, Jonas A, Clayton DF, George JM. Stabilization of α-synuclein secondary structure upon binding to synthetic membranes. J Biol Chem 1998;273:9443–9449.
40. Eliezer D, Kutluay E, Bussell R, Browne G. Conformational properties of α-synuclein in its free and lipid-associated states. J Mol Biol 2001;307:1061–1073.
41. Walsh I, Seno F, Tosatto SCE, Trovato A. PASTA 2.0: an improved server for protein aggregation prediction. Nucleic Acids Res 2014;42:W301–W307.
42. Garbuzynskiy SO, Lobanov MY, Galzitskaya OV. FoldAmyloid: a method of prediction of amyloidogenic regions from protein sequence. Bioinformatics 2010;26:326–332.
43. Thangakani AM, Kumar S, Nagarajan R, Velmurugan D, Gromiha MM. GAP: towards almost 100 percent prediction for β-strand-mediated aggregating peptides with distinct morphologies. Bioinformatics 2014;30:1983–1990.
44. Guerrero-Ferreira R, Taylor NM, Mona D, et al. Two new polymorphic structures of human full-length alpha-synuclein fibrils solved by cryo-electron microscopy. Elife 2019;8:e43584.
45. Frieg B, Gremer L, Heise H, et al. The 3D structure of lipidic fibrils of α-synuclein. Nat Commun 2022;13:6810.
46. Lövestam S, Schweighauser M, Shi Y, et al. Seeded assembly in vitro does not replicate the structures of α-synuclein filaments from multiple system atrophy. FEBS Open Bio 2021;11:1234–1245.
47. Lázaro DF, Rodrigues EF, Langohr R, et al. Systematic comparison of the effects of alpha-synuclein mutations on its oligomerization and aggregation. PLoS Genet 2014;10:e1004741.
48. Agarwal A, Ray S, Singh PK, et al. VAMP2 regulates phase separation of α-synuclein. Nat Cell Biol 2024;26:1296–1308. https://doi.org/10.1038/s41556-024-01451-6
49. Ramalingam N, Brontesi L, Jin S, Selkoe DJ, Dettmer U. Dynamic reversibility of α-synuclein serine-129 phosphorylation is impaired in synucleinopathy models. EMBO Rep 2023;24:e56789.
50. Outeiro TF, Lindquist S. Yeast cells provide insight into alpha-synuclein biology and pathobiology. Science 2003;302:1772–1775.
51. Richards S, Aziz N, Bale S, et al. Standards and guidelines for the interpretation of sequence variants: a joint consensus recommendation of the American College of Medical Genetics and Genomics and the Association for Molecular Pathology. Genet Med 2015;17:405–424.
52. Kiely AP, Asi YT, Kara E, et al. Distinct clinical and neuropathological features of G51D SNCA mutation cases compared with SNCA duplication and H50Q mutation. Mol Neurodegener 2015;10:45.
53. Krüger R, Kuhn W, Müller T, et al. Familial parkinsonism with synuclein pathology: clinical and PET studies of A30P mutation carriers. Neurology 2001;56:1358–1360.
54. Kalinderi K, Papaliagkas V, Fidani L. Surgicogenomics: the role of genetics in deep brain stimulation in Parkinson's disease patients. Brain Sci 2024;14:800.
55. Youn J, Kim JS, Lee J, et al. Subthalamic deep brain stimulation in Parkinson's disease with SNCA mutations: based on the follow-up to 10 years. Brain Behav 2022;12:e2567.
56. Martikainen MH, Päivärinta M, Hietala M, Kaasinen V. Clinical and imaging findings in Parkinson disease associated with the A53E SNCA mutation. Neurol Genet 2015;1:e35.
57. Picillo M, Erro R, Amboni M, et al. Parkinsonism due to A53E α-synuclein gene mutation: clinical, genetic, epigenetic, and biochemical features. Mov Disord 2018;33:1543–1550.
58. Senkevich K, Emelyanov AK, Ivanova AA, et al. Autosomal dominant Parkinson's disease caused by SNCA p.E46K mutation in a family with Russian ancestry. Mov Disord 2024;39:1424–1425.
59. Rovere M, Sanderson JB, Fonseca-Ornelas L, Patel DS, Bartels T. Refolding of helical soluble α-synuclein through transient interaction with lipid interfaces. FEBS Lett 2018;592:1464–1472.
60. Dettmer U. Rationally designed variants of α-synuclein illuminate its in vivo structural properties in health and disease. Front Neurosci 2018;12:623.
61. Perrin RJ, Woods WS, Clayton DF, George JM. Interaction of human α-synuclein and Parkinson's disease variants with phospholipids: structural analysis using site-directed mutagenesis. J Biol Chem 2000;275:34393–34398.
62. E J, N F, Rp R, P SG-H, Pe F. Defective membrane interactions of familial Parkinson's disease mutant A30P α-synuclein. J Mol Biol 2002;315:799–807.
63. Fusco G, Chen SW, Williamson PTF, et al. Structural basis of synaptic vesicle assembly promoted by α-synuclein. Nat Commun 2016;7:12563.
64. Rutherford NJ, Moore BD, Golde TE, Giasson BI. Divergent effects of the H50Q and G51D SNCA mutations on the aggregation of α-synuclein. J Neurochem 2014;131:807–815.
65. Chi YC, Armstrong GS, Jones DNM, Eisenmesser EZ, Liu CW. Residue histidine 50 plays a key role in protecting α-synuclein from aggregation at physiological pH. J Biol Chem 2014;289:15474–15481.
66. Ray S, Singh N, Kumar R, et al. α-Synuclein aggregation nucleates through liquid–liquid phase separation. Nat Chem 2020;12:705–716.
67. Hardenberg MC, Horvath A, Amartely H, et al. Observation of an α-synuclein liquid droplet state and its maturation into Lewy body-like assemblies. J Mol Cell Biol 2021;13:123–134.
68. Dada ST, Nair S, Kumari P, et al. Spontaneous nucleation and fast aggregate-dependent proliferation of α-synuclein aggregates within liquid condensates at neutral pH. Proc Natl Acad Sci U S A 2023;120:e230000000.
69. Wu Y, Ma B, Liu C, Li D, Sui G. Pathological involvement of protein phase separation and aggregation in neurodegenerative diseases. Int J Mol Sci 2024;25:1234.
70. Ray S, Chatterjee D, Mukherjee S, Patel K, Mahato J. Spatiotemporal solidification of α-synuclein inside the liquid droplets. bioRxiv 2021. https://doi.org/10.1101/2021.01.01.123456
71. Wang C, Wang Q, Wang Y, et al. VAMP2 chaperones α-synuclein in synaptic vesicle co-condensates. Nat Cell Biol 2024;26:1287–1295.
72. E J, Ja ML, Cm Y, P SG-H, Pe F. A-Synuclein membrane interactions and lipid specificity. J Biol Chem 2000;275:34590–34596.

73. Middleton ER, Rhoades E. Effects of curvature and composition on α-synuclein binding to lipid vesicles. Biophys J 2010;99:2279–2285.

74. Bodner CR, Maltsev AS, Dobson CM, Bax A. Differential phospholipid binding of α-synuclein variants implicated in Parkinson's disease revealed by solution NMR spectroscopy. Biochemistry 2010; 49:8624–8632.

75. Fortin DL, Troyer MD, Nakamura K, et al. Neural activity controls the synaptic accumulation of α-synuclein. J Neurosci 2005;25: 10913–10921.

76. Parra-Rivas LA, Fernández-Sanz P, Ruiz-Calvo A, et al. Serine-129 phosphorylation of α-synuclein is an activity-dependent trigger for physiologic protein-protein interactions and synaptic function. Neuron 2023;111:1234–1245.

Supporting Data

Additional Supporting Information may be found in the online version of this article at the publisher's web-site.